JOURNAL OF GEOPHYSICAL RESEARCH, VOL. 90, NO. A2, PAGES 1205–1216, FEBRUARY 1, 1985

Magnetotail Energy Storage and Release During the CDAW 6 Substorm Analysis Intervals

D. N. BAKER,[1] T. A. FRITZ,[1] R. L. MCPHERRON,[2] D. H. FAIRFIELD,[3] Y. KAMIDE,[4] AND W. BAUMJOHANN[5]

A primary goal of the Coordinated Data Analysis Workshop (CDAW) 6 has been to study the flow of energy from the solar wind through the magnetosphere and in so doing to examine the role of magnetotail storage and rapid dissipation of this energy during magnetospheric substorms. The chosen intervals for CDAW 6 analysis (March 22 and March 31 to April 1, 1979) are well suited for such studies since spacecraft were situated upstream (IMP 8 and ISEE 3) to measure magnetospheric energy input from the solar wind and spacecraft were also located in the magnetotail (ISEE 1, 2) and the midnight sector at geostationary orbit (76-059, 77-007, GEOS 2, GOES 3) during several of the substorm periods. Using solar wind, magnetotail, and geostationary particle and field data, as well as ground-based information, we present the evidence for enhanced solar wind–magnetosphere coupling and concomitant increases of stored magnetotail energy. Clear examples of energy storage are found prior to the 1055 and 1435 UT substorms of March 22, as well as the 0250 UT and 2250 UT substorms on April 1 and March 31, respectively. In these cases we estimate the total energy increase in the tail prior to the substorm onsets, and we estimate the dissipation rate of this energy during the substorms themselves. Typical total energy increases in the tail ($\gtrsim 5 \times 10^{22}$ ergs) appear to be more than adequate to supply the substorm energy dissipation inferred from ground-based and spacecraft observations.

INTRODUCTION

The Coordinated Data Analysis Workshop (CDAW) is a concept that grew out of the International Magnetospheric Study (IMS) program. The fundamental notion underlying the CDAW has been to pool data from a wide variety of spacecraft and ground-based sources for limited time intervals and to then perform very detailed correlative analyses of these data, usually with fairly limited physical problems in mind. Several of the CDAW efforts have investigated localized regions or else have dealt primarily with microphysical aspects of space physics.

The CDAW 6 effort established quite ambitious and truly global goals from its outset [*McPherron and Manka*, this issue]. The primary expressed goal of CDAW 6 can be stated as follows: to trace the flow of energy from the solar wind through the magnetosphere to its ultimate dissipation by substorm processes. It is obvious that this undertaking would require a large observational data base both in space and on the ground. Fortuitously, the combinations of spacecraft and ground arrays available during the IMS have been admirably suited to this task.

Our specific goal in the present study is to examine the evidence for the storage of solar wind energy in the magnetotail prior to substorm expansion phase onsets. We also wish to examine the details of the release and dissipation of this stored energy subsequent to substorm expansion onset. Of particular interest is the determination, in individual substorm cases, of the time delays between the loading of energy into the magnetospheric system and the subsequent unloading of this energy. The objective of such analyses is to determine characteristic magnetospheric time scales in the case of the several more or less arbitrarily chosen CDAW 6 substorm events for which virtually no disagreement exists as to substorm characteristics, onset times, the maximum epoch, etc.

In the process of examining the evidence for storage and sudden release of energy throughout the selected CDAW 6 intervals, we must nearly of necessity follow energy flow from the solar wind through the outer magnetosphere and into the ionosphere and/or ring current. Thus our present study subsumes many of the overall objectives of the CDAW 6 program.

Considerable prior work has established that enhanced solar wind–magnetosphere energy coupling occurs during episodes of southward interplanetary field and increased solar wind speed [e.g., *Nishida*, 1983, and references therein]. Following increased energy coupling, many observables can be invoked as qualitative and quantitative measures of increased energy storage in the earth's magnetotail. Among these are increased magnetic energy density in the magnetotail lobes, increasingly taillike field near geostationary orbit, and systematic changes in energetic particle distributions at $\sim 6.6\ R_E$ [cf. *McPherron*, 1972; *Baker et al.*, 1981; *Fairfield et al.*, 1981]. The dissipation of energy during substorms can be directly adduced by the examination of ionospheric and ring current parameters and by the in situ observation of hot plasmas and energetic particle populations accelerated by substorm processes.

The observational tools employed here include spacecraft in the upstream solar wind (IMP 8, ISEE 3), spacecraft in the magnetotail (ISEE 1, 2), and several geostationary spacecraft (1976-059, 1977-007, GEOS 2, GOES 2, GOES 3, GMS, and SCATHA). Of particular further importance are ground-based data (magnetograms) and ionospheric parameters derived from these data. As will be seen below, we rely particularly upon the results of CDAW 6 modeling efforts which provide some of the best available estimates of energy dissipation terms such as the ionospheric Joule heating rate and total magnetospheric "energy output" (U_T).

OVERVIEW OF CDAW 6 ANALYSIS INTERVALS

As discussed by *McPherron and Manka* [this issue], the two intervals chosen for analysis in CDAW 6 (0600–2000 UT on March 22 and 1200–0600 UT on March 31 to April 1, 1979)

[1] Los Alamos National Laboratory, University of California, Los Alamos, New Mexico.
[2] University of California, Los Angeles.
[3] NASA Goddard Space Flight Center, Greenbelt, Maryland.
[4] Kyoto Sangyo University, Japan.
[5] Institut für extraterrestrische Physik, Max-Planck-Institut für Physik and Astrophysik, Garching, Federal Republic of Germany.

Paper number 4A0797.
0148-0227/85/004A-0797$05.00

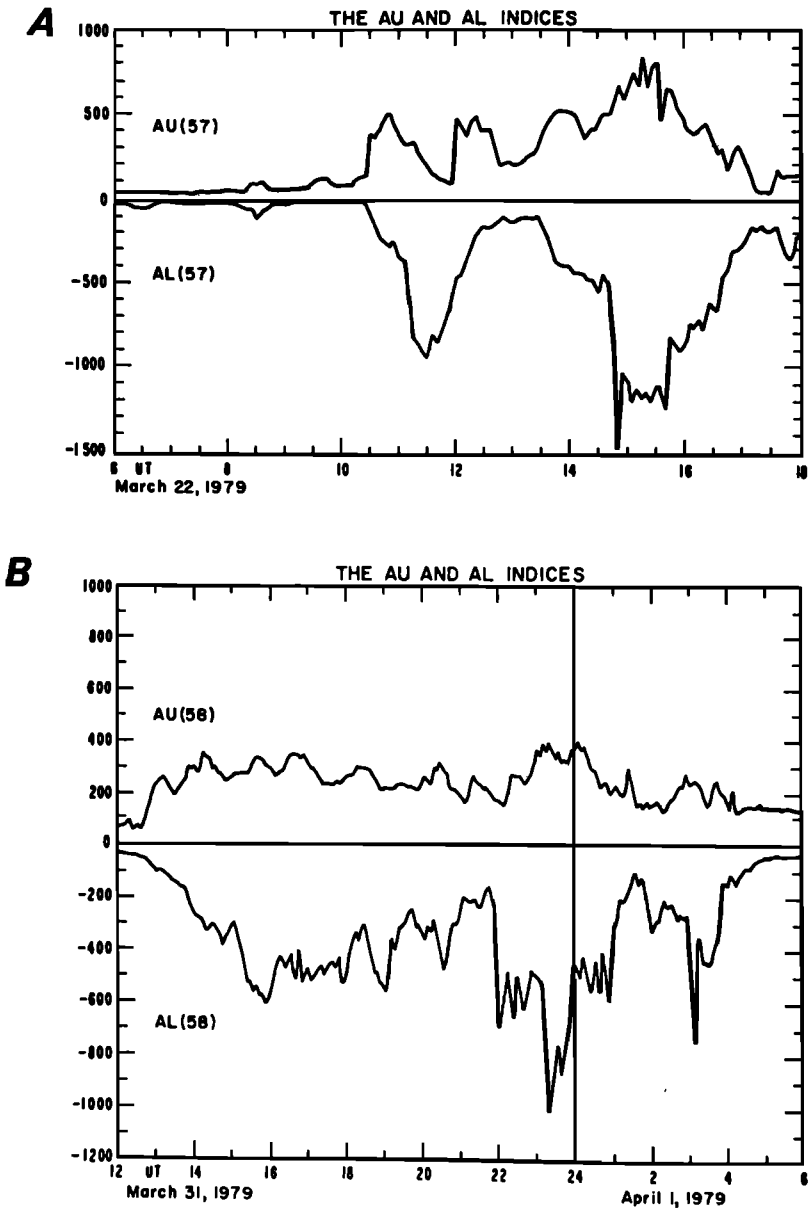

Fig. 1. The *AU* and *AL* indices computed for the CDAW 6 analysis intervals. (*a*) The *AU*(57) and *AL*(57) indices for 0600–1800 UT on March 22, 1979. (*b*) The *AU*(58) and *AL*(58) indices for 1200–0600 UT on March 31 to April 1, 1979.

were very different in the nature of their geomagnetic activity. The March 22 interval, although encompassing a moderate geomagnetic storm (*Dst* ~ -70 nT), basically consisted of two discrete, "isolated" substorm events. By way of contrast, the March 31 to April 1 interval was characterized by nearly continuous geomagnetic disturbance, and identification of individual substorm onsets in this interval is much more difficult.

As mentioned in the introduction, the CDAW 6 analysis effort relied heavily on observational data base resources obtained under the auspices of the IMS. As a result, unprecedented degrees of geophysical coverage were available both in space and on the ground. In particular, large numbers of ground-based magnetometer chains were available [*Kamide et al.*, 1983; *Kroehl and Kamide*, this issue], from which greatly improved geomagnetic indices were derived. Figure 1, for example, shows the *AU* and *AL* indices derived from 57 and 58 different auroral magnetometer stations for March 22 and March 31, repsectively [*Kroehl and Kamide*, this issue].

Figure 1 illustrates the distinctly different geomagnetic activity character of March 22 and March 31 discussed above. In the upper part of the figure, two major substorm intervals were seen commencing around 1100 UT and 1430 UT on March 22 which are characterized by sudden increases in the *AL* intensity. As described by *McPherron and Manka* [this issue], the wealth of CDAW 6 data available (Pi 2 records, particle data in the tail, magnetic signatures at 6.6 R_E, etc.) allow very precise and unambiguous determination of the substorm onsets: 1055 UT and 1436 UT.

The lower part of Figure 1 shows the continuously disturbed conditions on March 31. This second interval has been examined in many respects, but it has not received the extremely close scruitiny that has been accorded to the March 22 interval. Nonetheless, several substorm onsets (or, more properly, intensifications) can be discerned in the *AL* trace of Figure 1, and we will discuss several of these substorm events in some detail later in this paper.

Of special note for our purposes here will be numerous geostationary platforms, and relevant positional information

for these spacecraft is summarized in Table 1. In addition to these measurements at 6.6 R_E, we utilize data from ISEE 1, 2, and 3 plus IMP 8. Figure 2 shows the positions of these latter high-altitude spacecraft in an x-y plane projection for the intervals of interest: March 22 (day 81), 0600–2000 UT, and March 31 to April 1 (day 90–91), 1200–0600 UT. Nominal magnetopause and bow shock positions are also illustrated, but these boundary positions are highly variable, in reality, for the CDAW time periods (B. Wilken et al., unpublished manuscript, 1984).

In addition to the traditional indices of geomagnetic activity (*AE*, *Dst*, *ASYM*), several other parameters have also proven very valuable for our present analyses. As described by *Kamide and Baumjohann* [this issue], the extensive set of CDAW magnetometer chain data has allowed excellent determinations of global ionospheric electric fields and currents, field-aligned currents, and Joule heat production rates at high latitudes. The latter quantity, namely, the Joule heat rate, in particular has proven useful and convenient for our correlative work here. We also utilize many of the deep-space parameters described in the introduction to enhance our correlative capabilities (e.g., particle injections at 6.6 R_E). Finally, in an attempt to consider the entire magnetospheric energy output, we also examine the U_T parameter [*Akasofu*, 1981; *Baker et al.*, 1983], which considers both auroral and ring current dissipation terms. This parameter was computed for the CDAW 6 data intervals and was placed on the data base in the form of 5-min average values.

OBSERVATIONS

In this section we will discuss separately the March 22 and March 31 intervals. Several discrete substorm intervals will be examined in order to discern the nature of the magnetotail energy loading-unloading characteristics.

The March 22, 1979, Interval

Figure 3 presents an overview of the period from 0600 to 1800 UT on March 22, 1979. The upper two panels show interplanetary data from IMP 8, specifically the solar wind speed V_{SW} and the interplanetary magnetic field (IMF) B_z component. These parameters have been discussed in some detail by *McPherron and Manka* [this issue], and these authors also show the variation of other parameters such as solar wind density and total IMF magnitude. The primary features to note in the upper panels of Figure 3 are (1) the large increases in V_{SW} and B_z at ~0826 UT, when an interplanetary shock wave passed the magnetosphere (B. Wilken et al., unpublished manuscript, 1984) and then initiated a storm sudden commencement, and (2) the strong southward turnings of B_z at ~1010 UT and ~1310 UT following long periods of strong northward B_z.

As seen in the third panel of Figure 3, each southward turning of B_z initiated strong substorm activity as measured by *AE*(57). We will further examine the variations of *AE* below.

TABLE 1. Geostationary Orbit Spacecraft Examined in Study

Spacecraft	Longitude (Geographical)	Latitude (Magnetic)
1976-059	70°W	11°
1977-007	135°W	4.5°
GOES 3	135°W	4.5°
GEOS 2	30°E	−2.0°

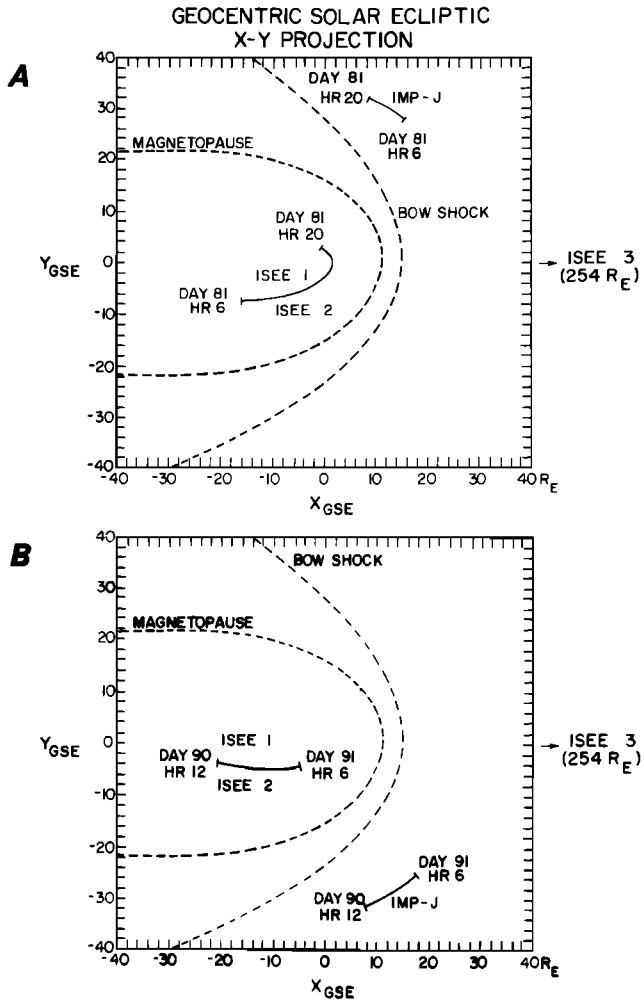

Fig. 2. The X-Y plane projections of the positions of ISEE 1, 2, and 3 and IMP 8 for (*a*) March 22 and (*b*) March 31 to April 1, 1979.

The bottom two panels of Figure 3 show near-magnetotail data from ISEE 2. As is evident from the low tail field strength (fourth panel) and relatively high plasma number density (fifth panel) prior to 1055 UT, ISEE 2 was predominantly in the plasma sheet before the first substorm expansion onset. At the time of the 1055 UT substorm, ISEE 2 generally observed large field increases and density decreases indicative of entrance into the tail lobes.

Specific treatments of the ISEE 1 and 2 observations in the tail around 1100 UT are given elsewhere [*McPherron and Manka*, this issue; T. A. Fritz et al., unpublished manuscript, 1984; *Paschmann et al.*, this issue]. The point to be gleaned from Figure 3 is that events in the tail in this case were well correlated with substorm onset and followed the beginning of enhanced energy input to the magnetosphere by ~45 min.

Note the relatively smooth, rapid increase of $|\mathbf{B}|$ at ISEE 2 after ~1200 UT. This trend, of course, is due to the inward trajectory of ISEE 2 which took it to low geocentric radial distances toward the end of the CDAW 6 interval (cf. Figure 2). Nonetheless, a plasma sheet "thinning" event appeared to be present between 1400 and 1500 UT in association with the second substorm event, and we will examine this feature further below.

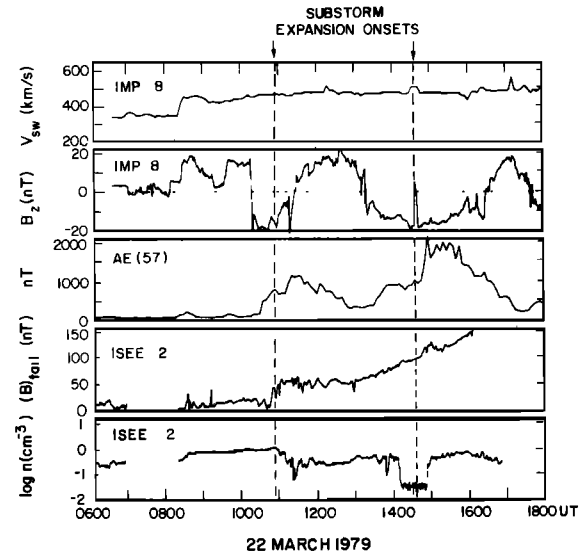

Fig. 3. Overview of observed conditions between 0600 and 1800 UT on March 22, 1979. From top to bottom panels: solar wind speed (IMP 8); IMF B_z component (IMP 8); the AE(57) index; tail field strength (ISEE 2); and the plasma number density in the magnetotail (ISEE 2).

Figure 4 shows more specific observations for the 1055 UT substorm event. The upper panel repeats the IMF B_z profile (as a measure of solar wind–magnetosphere coupling), the AE(57) plot is shown in the middle panel as a measure of geomagnetic activity, and the counting rate for >30-keV electrons at 6.6 R_E is shown in the third panel. The evident relationships seen in the data are that B_z turned southward at ~1010 UT. Approximately 10–15 min later (~1020 UT) the AE(57) index began to increase greatly and reached values in excess of 700 nT shortly before the identified substorm expansion onset. The energetic particle fluxes at 6.6 R_E showed a weak decrease at ~1030 UT and at ~1035 UT began a rapid, and nearly total, dropout that persisted until the substorm expansion at 1055 UT (T. A. Fritz et al., unpublished manuscript, 1984).

Note several features in Figure 4. First, the IMF was exhibiting a significant "northward turning" at the time of expansion onset. The role of this feature in the possible triggering of the substorm onset [cf. *Rostoker*, 1983] has yet to be assessed. Second, the AE index was nearly constant, or even decreasing, at the time of the expansion onset. This is due to a dramatic decrease in AU at the onset of the substorm, which is characterized by the sudden increase in the westward electrojet in the midnight sector [*Clauer and Kamide*, this issue]. Third, we note that in association with this feature in AE, however, the energetic particle fluxes recovered to their predropout level at ~1055 UT and did not increase above that level [cf. *Baker et al.*, 1982*a*, *b*] until ~1104 UT. Interestingly, it was at this latter time that AE(57) exhibited a further large increase.

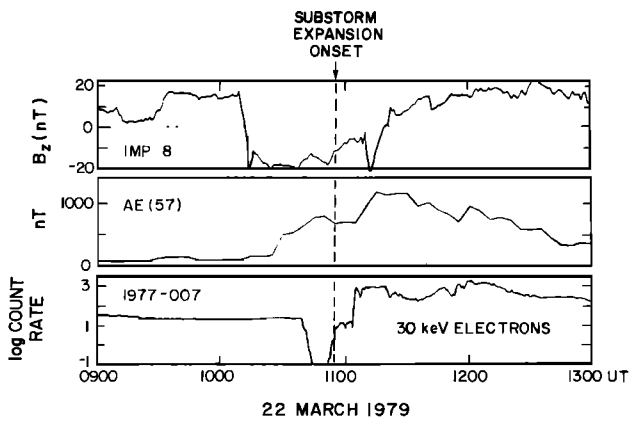

Fig. 4. Detailed observations surrounding the March 22, 1055 UT, substorm expansion onset. (*a*) The IMF B_z component (cf. Figure 3) for 0900–1300 UT. (*b*) The AE(57) index for 0900–1300 UT. (*c*) The counting rate for >30-keV electrons measured at spacecraft 1977-007 (6.6 R_E, ~135°W).

Past convention would identify the increase in AE (between 1020 and 1055 UT) and the electron flux dropout at 6.6 R_E as substorm growth phase features [*McPherron*, 1972; *Baker et al.*, 1981]. During this period, energy is extracted from the solar wind and is added to the magnetotail in the form of enhanced magnetic field energy density in the tail lobes. The increased magnetic field is due to greatly increased cross-tail currents in the near-tail midplane. Thus it would be expected in this picture that very taillike magnetic fields would be seen in the plasma sheet at near-earth, local midnight positions during the growth phase interval. Figure 5 shows explicitly the development of the magnetic field inclination θ_B measured at GOES 3. The angle θ_B is defined as the field colatitude in a dipolar coordinate system. A dipole field at the location of GOES 3 would have $\theta_B \sim 10°$ (i.e., twice the magnetic latitude of the spacecraft). A taillike field, that is, a field more nearly parallel to the magnetic equatorial plane, would have $\theta_B \rightarrow 90°$.

Figure 5 shows that θ_B at GOES 3 (~0130 LT) began to increase markedly at ~1020 UT. It reached values $\gtrsim 60°$ at ~1050 UT and rapidly diminished back to nearly dipolar values at precisely the substorm onset time, indicating that the GOES data confirm the expectation of very taillike field at 6.6 R_E between 1020 and 1055 UT. The rapid dipolarization of the field at GOES 3 between 1055 and 1105 UT is consistent with the rapid dissipation, i.e., unloading, of tail lobe energy

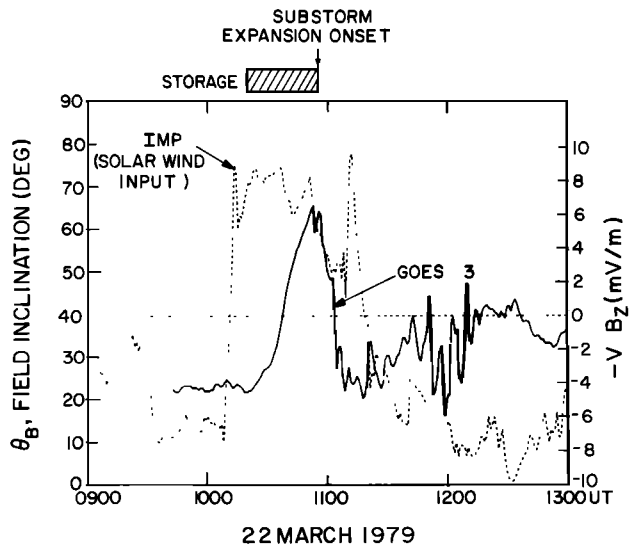

Fig. 5. A comparison of a solar wind–magnetosphere coupling function ($-VB_z$, dashed line) with the magnetic field inclination angle (θ_B, solid line) at geostationary orbit for the period 0900–1300 UT on March 22. The θ_B parameter shows a very taillike field development from 1020 to 1055. This is a classic substorm growth phase signature and is indicative of the dominance of loading of energy into the magnetotail.

and the diversion of the cross-tail currents through the auroral ionosphere.

The dotted line in Figure 5 shows a measure of solar wind energy input to the magnetosphere, namely $-VB_z$ (see, for example, *Nishida* [1983]). In the "half-wave rectifier" picture of magnetospheric response to the solar wind, energy coupling would have greatly increased (due to dayside reconnection) at ~1010 UT, i.e., when $-VB_z$ went to positive values. This is well supported by the data, since θ_B began to increase greatly (as did *AE*(57) in Figure 4) at a time ~10 min following the "turn-on" of the rectified solar wind energy input. Figure 5 also shows the relationship of the decrease in $-VB_z$ and the substorm expansion onset, although $-VB_z$ increased again at 1105 UT.

Neither θ_B nor *AE* is a true measure of magnetospheric energy dissipation, and thus to carry out our objectives we need to examine parameters explicitly related to ionospheric and ring current dissipation terms. Figure 6 shows the total Joule heat production rate (solid line) for the period 0900–1300 UT on March 22; see *Kamide et al.* [1983] for a description of the derivation. The dotted line is again the magnetospheric energy coupling function $-VB_z$.

A relatively modest increase in the total Joule heat production rate was seen from ~1020 UT to ~1105 UT, and a similar level was again seen after ~1240 UT. In contrast, a huge increase in the Joule heat rate was seen between 1105 and ~1230 UT. *Clauer and Kamide* [this issue] and *Kroehl and Kamide* [this issue] have shown that the period prior to ~1055 UT on March 22 was characterized by the *DP* 2-type current system, i.e., a twin-cell polar cap convection pattern. After ~1055 UT an intense *DP* 1 current system, centered at approximately the 0200 LT meridian, dominated the ionospheric current and the Joule heat production pattern. Thus the conclusion in this case is rather clear (cf., for example, *Baumjohann* [1983]): energy was added to the magnetosphere during the interval ~1015–1055 UT via coupling to the solar wind. The enhanced *DP* 2 polar cap current system was the "agent" of this coupling. Relatively small (in absolute magnitude), but global in spatial extent, dissipation was associated with this period preceding the major expansion of the substorm. Then, following 1100 UT, very large, intense dissipation of energy took place, and this dissipation was quite localized in the postmidnight sector of the magnetosphere-ionosphere system.

Figure 6 presents a remarkably clear demonstration of the relative roles of "directly driven" and "unloading" processes. The dotted curve in the figure is again the solar wind coupling function. Note that $-VB_z$, VB_s, ε, etc., all look virtually iden-

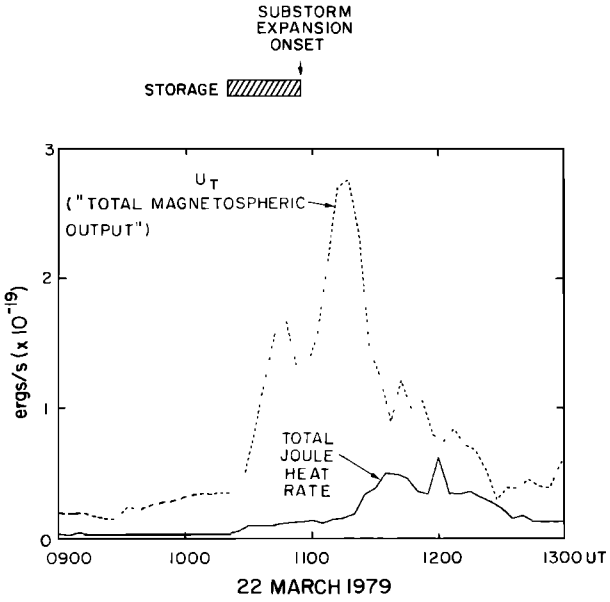

Fig. 7. A comparison of the total magnetospheric energy output (U_T, smoothed by a 15-min running average) and the total Joule heat production rate. The Joule heat is only a small fraction of the estimated U_T as discussed in the text.

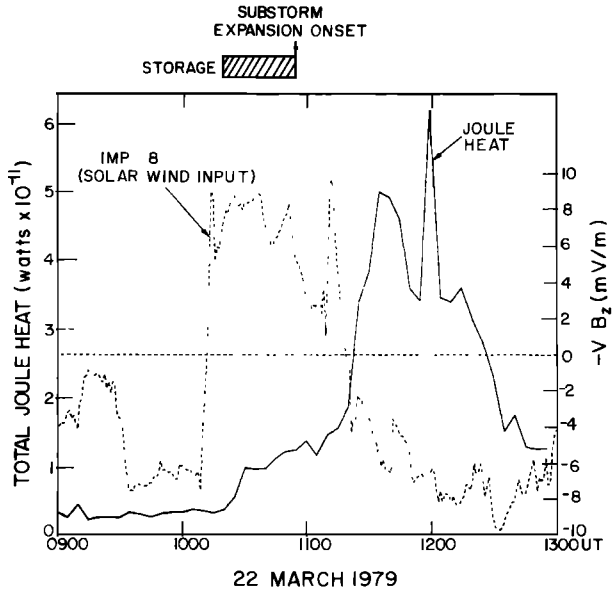

Fig. 6. A comparison of the solar wind coupling function ($-VB_z$, dashed line) with the computed total Joule heat production rate (solid line) for 0900–1300 UT on March 22. Note that $-VB_z$ was positive between 1010 UT and ~1110 UT while the Joule heat rate was largest after ~1110 UT.

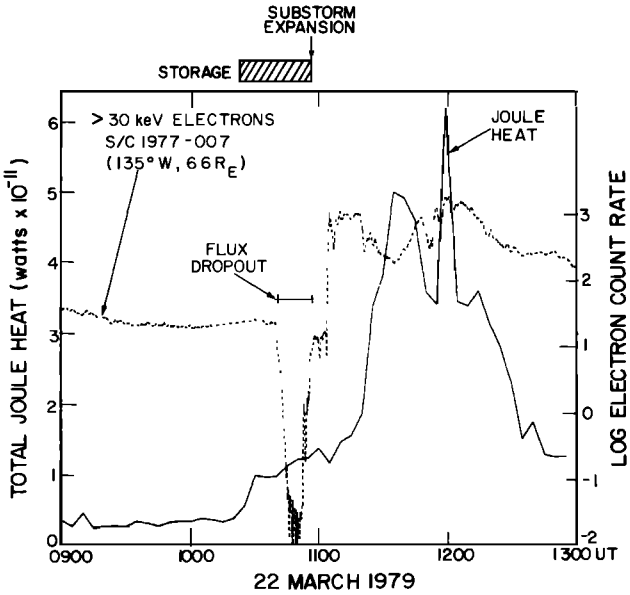

Fig. 8. A comparison of the total Joule heat rate (solid line) and the >30-keV electron counting rate at geostationary orbit. The electron flux dropout and other growth phase features at 6.6 R_E are well correlated with a low-level Joule heat dissipation rate while the large flux injection event (steplike increase at ~1110 UT) is associated with a very large Joule heat peak.

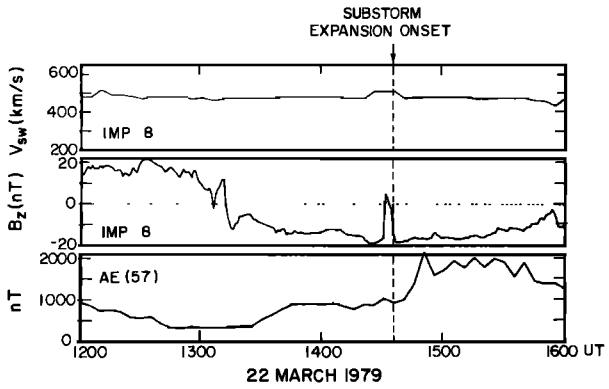

Fig. 9. A detailed plot of V_{SW}, B_z (IMF) and AE(57) for the interval 1200–1600 UT, on March 22, 1979. This period encompasses the 1436 UT substorm expansion onset.

tical in this case (see, for example, *Tsurutani et al.* [this issue]). The solid curve (Joule heat rate) can be regarded as a measure of the magnetospheric energy output rate. Figure 6 shows a nearly square wave energy input pulse from ~1010 UT to ~1110 UT after which energy input was turned off. With little delay (~10 min) the weak dissipation associated with loading the magnetospheric system was seen in the Joule heat curve. After the energy input was completely turned off, by far the largest Joule heat production rate was recorded (~1110–1230 UT). Based on these data, it is virtually beyond doubt that the energy for this intense phase of dissipation came from the magnetotail, not directly from the solar wind, and was of the classic *DP* 1 pattern usually associated with a localized nightside substorm "current wedge."

We have integrated the area under the Joule heat curve for the period 1010–1110 UT and from 1110 UT to 1230 UT. For the former, energy-loading interval the total dissipated Joule heat was $\sim 3.7 \times 10^{21}$ ergs. During the latter, energy-unloading interval the total dissipated Joule heat was $\sim 2.0 \times 10^{22}$ ergs. Thus the tail-unloaded energy dissipation during this event was over 5 times as much as the directly driven (loading) energy dissipation part.

It should be recognized that the Joule heat production rate is not the only form of substorm dissipation. Thus, as noted in the introduction, we have used another available CDAW 6 parameter, the "total" magnetospheric energy output function U_T [*Akasofu*, 1981]. It should be noted at the outset that U_T is only a rough estimate of ionospheric and ring current dissipation terms, and it has very definite limitations [see *Baker et al.*, 1983]. However, with these caveats in mind, Figure 7 shows a comparison of U_T (dotted line) with the Joule heat production rate (solid line). The figure shows that, indeed, the Joule heat rate is only about 10–50% of the estimated value of U_T. Nonetheless, U_T behaves in roughly the same way as the Joule heat curve and in fact looks almost identical to the AE profile in this period of time. Thus our conclusions drawn in the preceding part of this paper generally apply equally well whether AE, Joule heat, or U_T is used as a measure of magnetospheric "output."

Figure 8 illustrates the energetic particle measurements from spacecraft 1977-007 versus the Joule heat production rate. As seen in the figure, the particle fluxes recovered to their predropout value at the identified substorm onset time, but neither the >30-keV electron fluxes nor the Joule heat rate rose to very large values (above baseline levels) until several minutes after 1100 UT. The reason for these delays relative to the substorm onset time remains unclear (see T. A. Fritz et al., unpublished manuscript, 1984).

We now examine the second substorm on March 22. Figure 9 shows solar wind data (upper two panels) and AE(57) in an expanded fashion for the interval 1200–1600 UT. The substorm expansion onset has been well identified [*McPherron and Manka*, this issue] to be at 1436 UT. The IMF B_z went strongly and persistently southward at ~1310 UT as demonstrated in Figure 9; note again here, as in the 1055 UT substorm case, that B_z turned strongly positive just before the substorm onset and this may have played a role in the triggering of the substorm energy release [*Caan et al.*, 1978; *Rostoker*, 1983].

As is evident in Figure 9, AE(57) again rose gradually, but strongly, to values in excess of 800 nT after the IMF turned southward at 1310 UT. AE remained nearly constant at ~800 nT for about an hour (1340–1440 UT) before the substorm expansion phase began. At the expansion onset, AE increased rapidly and dramatically once more, reaching values at times in excess of 2000 nT.

Figure 10 is analogous to Figure 6 and compares the computed total Joule heat production rate (solid line) to a measure of the solar wind energy input, $-VB_z$. Figure 10 shows that the Joule heat rate increased gradually from a relatively low level at ~1325 UT. This increase began ~10–15 min after $-VB_z$ went strongly positive. The Joule heat rate then remained relatively constant at $\sim 3 \times 10^{11}$ W for about 1 hour (1340–1440 UT), and it increased very strongly after the identified substorm onset to a peak rate of nearly 18×10^{11} W (1.8×10^{19} ergs/s).

We identify the interval from ~1325 UT to 1436 UT as the traditional substorm growth phase. During this interval, solar wind energy was strongly coupled into the magnetosphere, and polar cap convective patterns were strongly enhanced [*Clauer and Kamide*, this issue]. The Joule heat rate of $\sim 3 \times 10^{11}$ W during this period is regarded as the dissipation associated with direct driving of the magnetosphere accompanying the loading of energy into the magnetotail.

The large enhancement of Joule heat dissipation after 1436 UT again represents the unloading of stored magnetotail

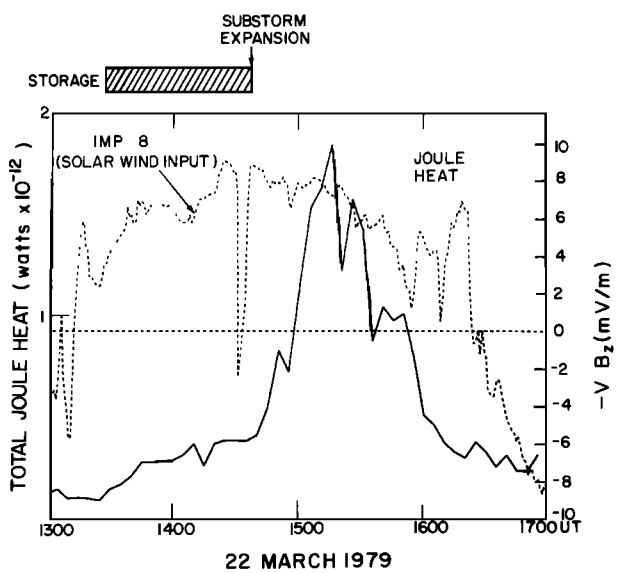

Fig. 10. Same as Figure 6 for the period 1300–1700 UT on March 22, 1979.

energy. In terms of a magnetotail substorm model, it represents the unloading of energy from the tail via a substorm current wedge which maps to a limited width of the plasma sheet. Although a substorm neutral line is likely the agent of production of this current wedge as in the case of the 1055 UT substorm [*McPherron and Manka*, this issue; T. A. Fritz et al., unpublished manuscript, 1984], ISEE 1 and 2 were not well situated to make in situ measurements of the neutral line properties in the 1436 UT substorm case (cf. Figure 2).

Note in Figure 10, in contrast to Figure 6, that $-VB_z$ remained strongly positive throughout most of this substorm interval rather than going negative at substorm expansion onset (as for the 1055 UT substorm). Thus energy continued to be supplied continuously to the magnetosphere even as energy was being rapidly unloaded from the tail during the interval 1435–1600 UT. This is consistent with the suggestion of *Clauer and Kamide* [this issue] and *Kamide and Baumjohann* [this issue] that during this second substorm on March 22, two current components, *DP* 1 and *DP* 2 types, coexisted.

As in the 1055 UT substorm case, it is instructive to make some estimates of the energy budget for the 1436 UT substorm. First, we estimate the rate of energy input from the solar wind. Many types of solar wind energy coupling estimates have been made in the past. Most of these suffer fundamentally from the problem of determining an "absolute" calibration. One of the more recent such parameters is ε [*Akasofu*, 1981], which has units of ergs per second and is given by $\varepsilon = VB^2 \sin^4 (\theta/2) l_0^2$. Using $l_0 = 7\ R_E$ and using the measured interplanetary data, a value of ε ranging between ~ 2 and $\sim 5 \times 10^{19}$ ergs/s from 1310 UT until ~ 1620 UT is obtained [*Tsurutani et al.*, this issue], and we use these estimates here recognizing the potential uncertainty in the values. To a good approximation, ε can be regarded as being $\sim 4 \times 10^{19}$ ergs/s throughout this whole interval, a very large energy input rate indeed.

Now let us consider energy dissipation rates. In Figure 10 the Joule heat rate appears relatively constant at $\sim 3 \times 10^{11}$ W (3×10^{18} ergs/s) for the intervals 1340–1440 UT and 1600–1630 UT. This was about 10% of the inferred energy input

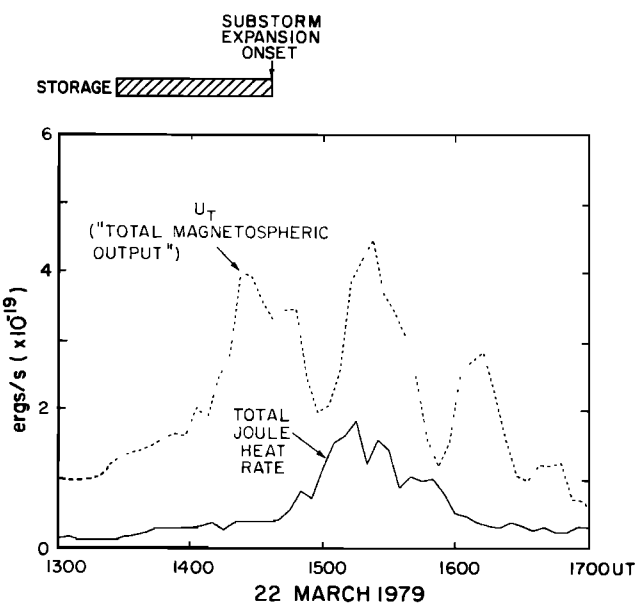

Fig. 11. Same as Figure 7 for the period 1300–1700 UT on March 22, 1979.

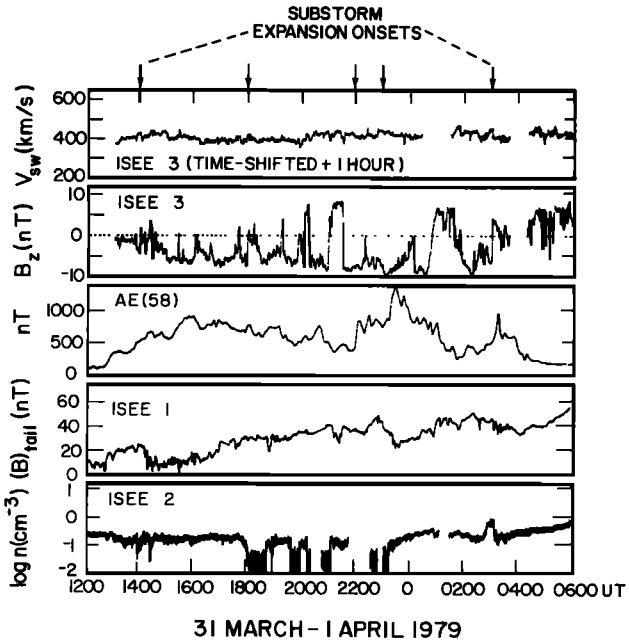

Fig. 12. A plot similar to Figure 3 for the second CDAW 6 analysis interval: 1200–0600 UT on March 31 to April 1, 1979. Note that the time-shifted ISEE 3 data have been used for interplanetary measurements and ISEE 1 tail field data are used.

rate and corresponds to the direct dissipation associated with the loading of solar wind energy into the magnetosphere. One possible assumption is that such a rate of dissipation (in Joule heating) went on throughout the interval $\sim$1340–1630 UT and was the baseline rate of Joule heat dissipation. Integrating this Joule heat rate over time (1340–1630) gives a total of 3×10^{22} ergs of dissipated energy.

The Joule heat dissipated in the *DP* 1 current wedge (from energy stored in the tail) can be estimated from the Joule heat peak in Figure 10. We have integrated the area under the curve (in excess of 3×10^{11} W) for the interval 1435 to 1600 UT. This integrated Joule heat is $\sim 5 \times 10^{22}$ ergs. There are indications (C. R. Clauer, personal communication, 1983) that the *DP* 2 currents became very large during the period of maximum dissipation shown in Figure 10. Thus we should be cautious in interpreting all of the dissipation in the peak of that figure as being due to *DP* 1 (unloading) effects. If we make such an assumption, however, then even for this case of strong, continuous driving of the magnetospheric system for several hours, the unloaded energy from the tail exceeded the "directly" dissipated ionospheric heat by a factor of ~ 2.

Again, with the Joule heat rate of Figure 10 we have not determined the entire magnetospheric energy output. In Figure 11 we plot (analogously to Figure 7) the estimated U_T for the period 1300–1700 UT. The values of U_T and the Joule heat rate again increase and decrease together reasonably well but, as in the 1055 substorm case, the Joule heat rate was only $\sim$10–30% of U_T. Note in Figure 11 that U_T tended to resemble *AE* or *AL* (Figure 1) in its time profile more than the Joule heat curve alone.

Recall that U_T became relatively large in Figure 7, as well as Figure 11, during the periods that we have identified as primarily energy storage intervals. As noted previously, because of limited magnetometer input, we do not have nearly the level of confidence in U_T that we have in the Joule heat curves, but nonetheless it is worthwhile to examine the vari-

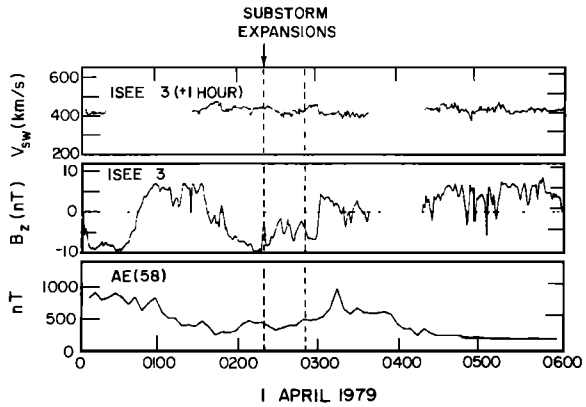

Fig. 13. Same as Figure 9 for the interval 0000–0600 UT on April 1, 1979.

ations of U_T in the overall context of solar wind–magnetosphere coupling. As we have described above, U_T tends to track the *AE* profile rather closely and therefore has a strong relationship to, and correlation with, auroral dissipation. Although U_T apparently greatly exceeds the Joule heat rate, considerable work remains to obtain the final intercalibration between the two quantities. Furthermore, it is highly likely that U_T, which is obtained from *Dst* and its time derivative, contains significant effects of the partial ring current, which in turn is due at least in part to the buildup of cross-tail currents (P. H. Reiff, personal communication, 1983). Thus the U_T increase during the energy storage phase of the March 22, 1979, substorms may result largely from the tail current (growth phase) contribution to the partial ring current. A very useful theoretical discussion of the relationship between the tail current systems and the asymmetric ring current is given by *Spiro and Wolf* [1984]. They show, for example, how the storm time compression of the magnetosphere contributes importantly to the ring current injection on March 22.

If we add up the energy input and energy output in the case of the 1435 substorm, we obtain some interesting numbers. Assuming a possible energy input given by ε for the period 1310–1630 UT gives

$$W_I = 4.5 \times 10^{23} \text{ ergs}$$

Adding up just the Joule heat (JH) dissipations determined above, we get

$$W_0(\text{JH: driven}) = 3 \times 10^{22} \text{ ergs}$$

$$W_0(\text{JH: unloading}) = 5 \times 10^{22} \text{ ergs}$$

giving a total Joule heat dissipation of $W_0(\text{JH}) \sim 8 \times 10^{22}$ ergs; this is a small fraction of the total W_I.

Even if we integrate the entire U_T curve from 1310 to 1630 UT, we get $W_0(U_T) \sim 2.5 \times 10^{23}$ ergs. Although these are rough numbers, we find with reasonable confidence that

$$W_0(\text{JH}) \ll W_I \qquad W_0(U_T) \sim \tfrac{1}{2} W_I$$

As discussed, for example, by *Baker et al.* [1981], the "missing" energy added to the magnetosphere must go into forms other than those accounted for in the ionospheric and ring current terms of U_T. Very likely, much of the input energy escapes down the tail in the form of plasmoid structures.

The March 31 to April 1, 1979, Interval

This second CDAW 6 interval was very different in character from the March 22 period. Figure 12 is analogous to Figure 3 and provides an overview of interplanetary, ground-based geomagnetic, and tail data for the period 1200 UT on March 31 to 0600 UT on April 1. The upper two panels show ISEE 3 data taken at $\sim$240 R_E upstream of the earth (cf. Figure 2). The data have been time-shifted by 1 hour in order to account for solar wind propagation delays. This time shift, determined empirically to give the best correlation with IMP 8 near the earth, is roughly consistent with the observed solar wind speed of 400 km/s ($\Delta t = \Delta x / V_{SW} \doteq (240\ R_E)/(400 \cdot \text{km/s})$) shown in the top panel of Figure 12.

Note that for the most part the IMF was strongly and persistently southward from $\sim$1400 UT until $\sim$0300 UT. Some notable periods of northward field, as at $\sim$2100 UT and 0045–0145 UT, were seen in the data, however. It was very likely this continually southward B_z which gave rise to the intense, continuous disturbance of auroral activity shown in Figure 12 by the *AE*(58) index. The times of several identified substorm expansion onsets are indicated at the top of the figure by the vertical arrows.

The lower two panels show ISEE field and plasma data, respectively, in the magnetotail. ISEE 1 and 2 were close to one another during this time, and in order to illustrate data of superior quality we plot magnetic field data from ISEE 1 and plasma number density from ISEE 2. Particularly between 1800 UT and $\sim$2300 UT, numerous entrances and exits of the ISEE pair between the tail lobe and plasma sheet were seen. Since those lobe–plasma sheet transitions were substorm related in several cases, we will examine some of these data more closely below.

Note in Figure 12 that a general increase in the IMF B_z occurred late in the CDAW interval. Associated with this, *AE*(58) diminished and appeared to exhibit a more "isolated" substorm behavior. In Figure 13 we show an expanded version of the V_{SW}, B_z, and *AE*(58) data for 0000–0600 UT on April 1. Close examination of the ground-based data, in fact, shows a double onset substorm expansion phase with onset times of $\sim$0220 UT and $\sim$0250 UT. These times are shown in Figure 13.

Note in Figure 13 that the IMF had been northward for nearly 1 hour (0045–0145 UT) prior to the substorm expansions. During this interval, *AE*(58) diminished substantially, and geomagnetic conditions quieted. B_z then went strongly southward again after $\sim$0145 UT, and *AE*(58) again

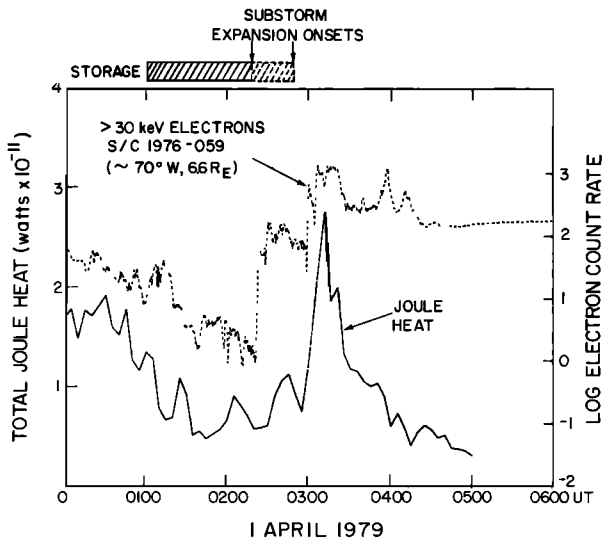

Fig. 14. Same as Figure 8 for 0000–0600 UT on April 1, 1979.

increased. A peak of AE activity was reached at ~0315 UT, well after the second substorm intensification at 0250 UT and at a time when B_z was northward.

Figure 14 illustrates >30-keV electron counting rates (dotted line) at geostationary orbit for the interval 0000–0600 UT. These data, from spacecraft 1976-059 at ~70°W, were taken in the premidnight sector at 6.6 R_E, a region ideally suited for the observance of substorm growth phase effects [e.g., *Baker et al.*, 1981]. As seen in the figure, shortly after 0100 UT the >30-keV electron fluxes began a rapid decrease. As in the 1055 UT substorm of March 22, this effect on April 1 can be taken as a growth phase signature. The flux drop was accompanied by an increasingly taillike field and other features indicative of strongly increased magnetotail energy storage. The hatched bar at the top of the figure shows the period of these growth phase effects.

A double step function increase in the energetic electron count rate was observed. The first at ~0220 UT corresponded to the first substorm expansion onset: an increase of flux by a factor of 2–3 over the predropout flux level was seen in this first step. The second increase in particle flux was also very sharp and occurred at ~0250 UT. This compared very well to the second identified expansion onset time, and this flux increased much higher in absolute intensity than the first event.

The solid line in Figure 14 shows the calculated total Joule heat rate. Prior to ~0130 UT the Joule heat rate appeared to be diminishing from prior periods of strong activity. The lowest levels of Joule heat production were seen early in the growth phase interval. Interestingly, only a relatively small increase in the Joule heat rate was seen in association with the first expansion onset (and particle injection) at 0220 UT. A very large peak in the Joule heat rate occurred in good time coincidence with the second injection event at 6.6 R_E following the 0250 UT expansion onset.

Figure 15 shows the relationship between solar wind energy input $-VB_z$ and magnetospheric energy dissipation (Joule heat rate). The plot is analogous to Figures 6 and 10. As in the March 22, 1055 UT, substorm example of Figure 6, the Joule heat dissipation rate was low between ~0130 UT and ~0300 UT on April 1 when the solar wind coupling parameter $-VB_z$ was high. Only after $-VB_z$ went negative (or near zero) was

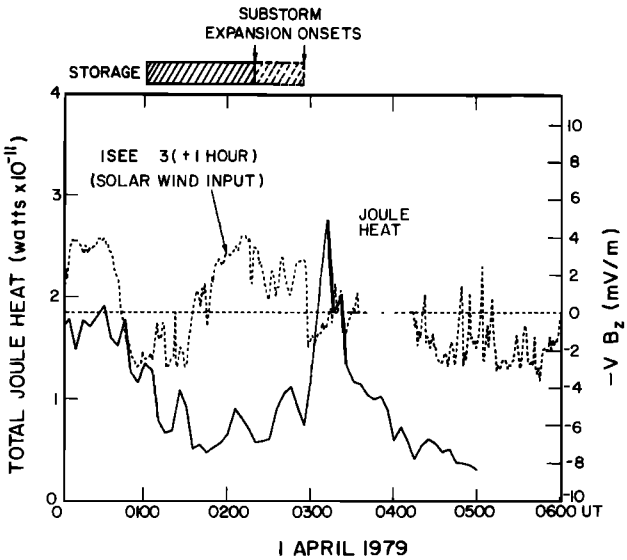

Fig. 15. Same as Figure 6 for 0000–0600 UT on April 1, 1979.

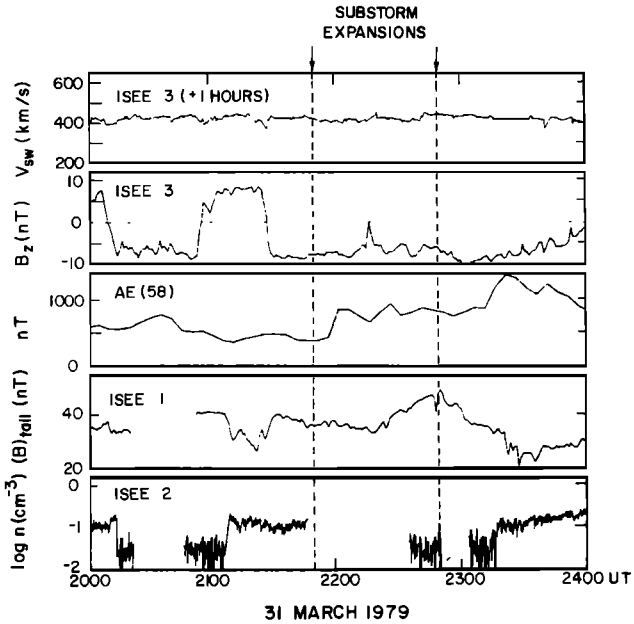

Fig. 16. An expanded portion of Figure 12 showing details of observations for substorm expansions at ~2150 and ~2250 UT on March 31, 1979.

the Joule heat rate large. Thus we again see a clear and distinct difference in the size, shape, and timing of the energy input function and the energy output function, thereby suggesting the very important role of magnetotail energy storage and subsequent sudden release.

As a final example of the importance of magnetotail energy storage in the CDAW 6 substorm events, we consider the period from 2000 to 2400 UT on March 31. A blowup of a section of Figure 12 for this period is shown here as Figure 16. Two extensive periods of strong southward IMF were seen in this interval, namely, 2010–2050 UT and 2125–2350 UT. A brief northward turning of the IMF occurred (without too much obvious effect) at ~2215 UT. Identification of substorm expansion onsets from the AE(58) time profile alone would be difficult, but the AL(58) (Figure 1*b*) and further ground-based data show much more evident onset features around 2150 and 2250 UT.

For our present purposes we concentrate on the substorm onset at 2250 UT. As seen in Figure 16, this onset was preceded by a long interval of southward IMF and, also, it occurred while ISEE 1 and 2 were in the magnetotail lobe (N.B. the low plasma number density and high tail field strength). In particular, note the large, rapid increase of tail field strength measured by ISEE 1 from ~2220 UT until ~2250 UT. At the time of the substorm expansion onset (i.e., 2250 UT), B_{tail} diminished rapidly from its peak value of ~50 nT back to its "baseline" lobe value of ~35 nT.

As seen in Figure 16, the variation of B_{tail} at ISEE 1 was not related to any variation of the solar wind speed (upper panel). We have also examined the solar wind density and find no correlated changes with the increase and decrease of B_{tail}. Therefore the solar wind dynamic pressure did not cause this change in the tail field, and we conclude that it was due to increased energy storage in the magnetotail lobes.

Having "clean" measurements of the lobe magnetic field strengths, we can conveniently make estimates of the energy storage and dissipation rates (see, for example, *Baker et al.* [1981] and *Fairfield et al.* [1981]). First of all we can estimate

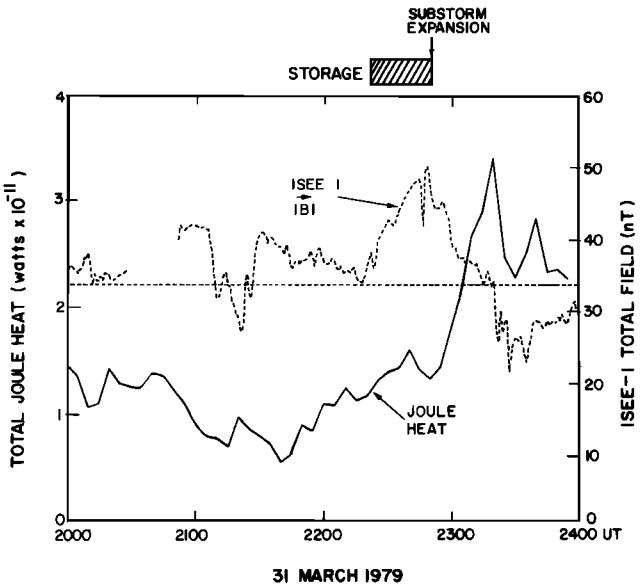

Fig. 17. A comparison of the total Joule heat production rate (solid line) and the magnetotail field strength (dashed line) between 2000 and 2400 UT on March 31. A large increase in B_{tail} was seen during a substorm growth phase in the interval 2215 to 2250 UT. The tail field rapidly diminished following the expansion phase onset at 2250 UT. The tail field rapidly diminished following the expansion phase onset at 2250 UT.

the change in magnetic energy density from the spacecraft data:

$$\delta w = \delta(B^2/8\pi) = 2\langle B\rangle \delta B/8\pi$$

For the case at hand,

$$\delta B = 15 \text{ nT} \qquad \langle B\rangle \sim 42 \text{ nT}$$

for which

$$\delta w \simeq 5 \times 10^{-9} \text{ erg/cm}^3$$

In order to make additional estimates we must estimate the effective tail volume involved. Assuming a cylindrical volume,

$$V = \pi r^2 L$$

and with very rough (and quite debatable) assumptions of

$$r \sim 15\ R_E \qquad L \sim 50\ R_E$$

we have

$$V \sim 9 \times 10^{30} \text{ cm}^3$$

Using the above results, we find that the total tail energy gain for the period 2220–2250 UT was

$$W_T \simeq \delta w \cdot V \sim 4.6 \times 10^{22} \text{ ergs}$$

Note in Figure 16 that B_{tail} rapidly decreased from 50 to ~35 nT between 2250 and 2315 UT. Thus we get that the power extracted from the stored magnetotail energy was

$$P_{tail} = W_T/\Delta t \sim 3.1 \times 10^{19} \text{ ergs/s}$$

For the period 2130–2330 UT, the power input ε from the solar wind was typically $\sim 3 \times 10^{18}$ ergs/s. Thus for a short period (2250–2315) after the substorm expansion the magnetotail gave up energy at a rate roughly 10 times the input rate. We thus conclude that magnetotail storage and sudden release must be considered as a very important effect under such circumstances.

Figure 17 shows the total Joule heat production rate (solid line) for the period 2000–2400 UT, while the dotted line shows the magnetotail field B_{tail} measured by ISEE 1. Based on our discussion above, we identify the period 2220–2250 UT as the period during which the storage process is dominant.

Between 2000 UT and ~2250 UT the total Joule heat rate averaged $\sim 1.5 \times 10^{18}$ ergs/s, which was about one half of the energy input rate ε which was $\sim 3 \times 10^{18}$ ergs/s. The Joule heat rate diminished considerably around 2100 UT when B_z went northward and ε dropped to near zero. A large peak in the Joule heat rate occurred following the substorm expansion onset at 2250 UT, and this was superimposed on the persisting background Joule heat curve. The peak Joule heat rate at 2315 UT of $\sim 3.5 \times 10^{18}$ ergs/s was comparable to the value of ε, and this does not even consider other contributions to U_T beside the Joule heating. Note the striking relationship between the decrease in B_{tail} and the increase in the Joule heat rate. These data make a strong further case for the role of magnetotail storage–sudden release in substorms.

Summary and Conclusions

In this paper we have examined on a case-by-case basis the relationship between energy input from the solar wind to the magnetosphere and, subsequently, the dissipation of this energy by substorm processes. The very clear pattern which emerges in each instance is that energy input was substantially enhanced when the IMF orientation turned southward. In clean north-to-south IMF transition examples of the sort studied here, the magnetosphere responded to this enhanced energy coupling in a very short time (10–15 min) with there then being a period of 30–60 min of relatively low level energy dissipation. This ½- to 1-hour interval of Joule heating, enhanced convection, etc., followed the classic pattern of the substorm growth phase [*McPherron*, 1972] and in every case examined corresponded to the "loading" of energy into the magnetotail.

By virtue of the extensive spacecraft and ground-based arrays available in the CDAW 6 analysis effort, we had very precise substorm expansion onset timing available for each of our case studies. We were thus able to distinguish clearly between preexpansion onset dissipation and postexpansion onset dissipation. In all cases, the dissipation after the expansive

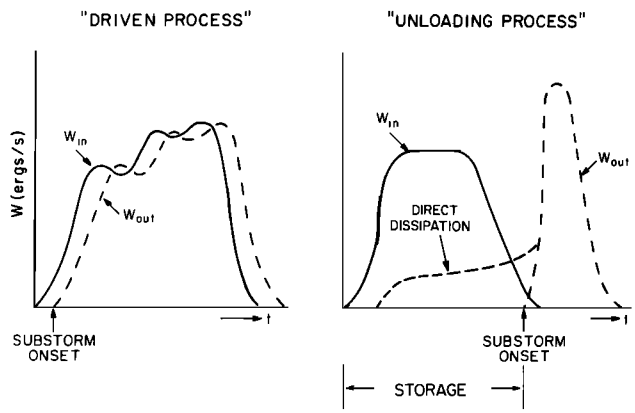

Fig. 18. An idealized illustration of the directly driven (left) and unloading (right) models of the relationship between magnetospheric energy input W_{in} and energy output W_{out}. As discussed in the text, the unloading model, with the allowance of a relatively low level of dissipation during the growth phase interval, fits the observations presented in this paper.

phase onset was substantially larger than during the period of primary energy storage.

Much of the controversy in substorm studies of late has been related to whether substorms are a driven or an unloading process. Recent thinking [e.g., *Baker et al.*, 1984] has emphasized that both driven and unloading processes must be considered. In Figure 18 we illustrate the two extreme viewpoints. The solid and long-dashed curves in this figure are taken from the paper by *Baker et al.* [1982*b*] and were adapted from *Akasofu* [1981]. In the extreme "driven" scenario the energy output of the magnetosphere, W_{out}, tracks the solar wind energy input W_{in} with great faithfulness (with perhaps a slight time delay). In this model there is no significant role of tail energy storage. In the extreme "unloading" model on the right, as shown by the solid and dashed lines, there is no significant dissipation of energy, W_{out}, until after energy has been loaded into the system, W_{in}, for of the order of 1 hour.

The results of the present study show that in fact neither extreme model is totally correct. However, every case examined here showed that magnetotail storage of energy was quite important to the substorm development. Furthermore, in none of the cases examined in our high time resolution analysis was there any detailed resemblance between the solar wind input profile and the magnetospheric output profile (cf. Figures 6, 10, 15, and 16). In all of these cases, energy was added to the magnetosphere for a substantial period (30–60 min) before the substorm onset occurred and very intense, localized dissipation began (*DP* 1 current system).

This study also demonstrates quite clearly, however, that magnetospheric energy dissipation is not negligible during the "growth phase" (energy loading) interval. Lower level, but very global, dissipation in *DP* 2 kinds of current systems accompany the increase of stored magnetotail energy. Our quantitative estimates indicate that the time-integrated total dissipation during the loading process is usually less (by a factor of 2–5) than the total dissipation during the unloading process. This ratio is highly variable.

The results of this study are most supportive of a model which modifies the unloading model of Figure 18 as shown by the short-dashed line. During the growth phase there is a long interval of low level, but significant, energy dissipation. This is a (*DP* 2) energy output that accompanies the global convection (in the polar cap) which loads energy into the magnetotail lobes. At substorm expansive phase onset there is a large intensification of the dissipation rate, and this corresponds to the unloading of energy from the tail. Thus both directly driven loading (growth phase) and nondriven unloading (expansive phase) processes play an important role in substorms depending on the different phases. As shown, for example, by the 1436 UT substorm case presented here (Figure 10), both the driven and unloading processes can, and do, go on concurrently in many instances.

The present study again illustrates in a very concrete way the important characteristic time constants of the magnetospheric substorm response to solar wind input. In nearly all the cases studied in this paper, there was a rapid, sharp southward IMF turning that initiated the substorm activity. About 10–20 min later, growth phase effects were seen in the *AE* index, in the field inclination at 6.6 R_E, in particle distribution functions, in total Joule heat, etc. Then, about one hour after the southward IMF turning, the substorm expansive phase itself occurred with strong enhancement of Joule heat production, particle injection events at 6.6 R_E, near-tail magnetic field dipolarization, etc. These results provide strong case study support for the statistical result of L. F. Bargatze et al. (unpublished manuscript, 1984) which showed two peaks in the impulse response function of the magnetosphere: one at ~20 min and one at ~60 min. Bargatze et al. suggested that the 20-min peak was the response time scale for directly driven substorm processes while the 60-min peak was the response time scale for magnetotail energy unloading processes.

Acknowledgments. The CDAW 6 activity has used extensively the facilities of the National Space Science Data Center at NASA Goddard Space Flight Center, and we thank James I. Vette and his organization for their efforts. Many other scientists have contributed their efforts to the interpretation of the CDAW 6 events and we acknowledge their collective contributions; we especially thank C. R. Clauer, J. H. King, P. H. Reiff, and L. F. Bargatze for their comments on this work. We also wish to thank R. H. Manka for his organizational efforts in making CDAW 6 the success it has become. Work at Los Alamos was done under the auspices of the U.S. Department of Energy. Y. Kamide was supported in part by the National Academy of Science under the Associateship Program and in part by the National Institute of Polar Research.

The Editor thanks B. Wilken and A. Nishida for their assistance in evaluating this paper.

REFERENCES

Akasofu, S.-I., Energy coupling between the solar wind and the magnetosphere, *Space Sci. Rev.*, *28*, 121, 1981.

Baker, D. N., E. W. Hones, Jr., P. R. Higbie, R. D. Belian, and P. Stauning, Global properties of the magnetosphere during a substorm growth phase: A case study, *J. Geophys. Res.*, *86*, 8941, 1981.

Baker, D. N., T. A. Fritz, B. Wilken, P. R. Higbie, S. M. Kaye, M. G. Kivelson, T. E. Moore, W. Studemann, A. J. Masley, P. H. Smith, and A. L. Vampola, Observation and modeling of energetic particles at synchronous orbit on July 29, 1977, *J. Geophys. Res.*, *87*, 5917, 1982*a*.

Baker, D. N., E. W. Hones, Jr., R. D. Belian, P. R. Higbie, P. R. Lepping, and P. Stauning, Multiple-spacecraft and correlated riometer study of magnetospheric substorm phenomena, *J. Geophys. Res.*, *87*, 6121, 1982*b*.

Baker, D. N., R. D. Zwickl, S. J. Bame, E. W. Hones, Jr., B. T. Tsurutani, E. J. Smith, and S.-I. Akasofu, An ISEE 3 high time resolution study of interplanetary parameter correlations with magnetospheric activity, *J. Geophys. Res.*, *88*, 6230, 1983.

Baker, D. N., S.-I. Akasofu, W. Baumjohann, J. W. Bieber, D. H. Fairfield, E. W. Hones, Jr., B. Mauk, R. L. McPherron, and T. E. Moore, Substorms in the magnetosphere, in *Solar Terrestrial Physics—Present and Future*, edited by K. Papadopoulos and D. Butler, chap. 8, NASA, Washington, D. C., 1984.

Baumjohann, W., Ionospheric and field-aligned currents in the auroral zone: A concise review, *Adv. Space Res.*, *2*, 55, 1983.

Caan, M. N., R. L. McPherron, and C. T. Russell, The statistical magnetic signature of magnetospheric substorms, *Planet. Space Sci.*, *26*, 269, 1978.

Clauer, C. R., and Y. Kamide, *DP* 1 and *DP* 2 current systems for the March 22, 1979, substorms, *J. Geophys. Res.*, this issue.

Fairfield, D. H., R. P. Lepping, E. W. Hones, Jr., S. J. Bame, and J. R. Asbridge, Simultaneous measurements of magnetotail dynamics by IMP spacecraft, *J. Geophys. Res.*, *86*, 1396, 1981.

Kamide, Y., and W. Baumjohann, Estimation of electric fields and currents from International Magnetospheric Study magnetometer data for the CDAW 6 intervals: Implications for substorm dynamics, *J. Geophys. Res.*, this issue.

Kamide, Y., H. W. Kroehl, B. A. Hausman, R. L. McPherron, S.-I. Akasofu, P. H. Reiff, A. D. Richmond, and S. Matsushita, Numerical modeling of ionospheric parameters from global IMS magnetometer data for the CDAW-6 intervals, *Rep. UAG-288*, 205 pp., World Data Center A for Sol.-Terr. Phys., Boulder, Colo., Nov. 1983.

Kroehl, E. W., and Y. Kamide, High-latitude indices of electric and magnetic variability during the CDAW 6 intervals, *J. Geophys. Res.*, this issue.

McPherron, R. L., Substorm related changes in the geomagnetic tail: The growth phase, *Planet. Space Sci.*, *20*, 1521, 1972.

McPherron, R. L., and R. H. Manka, Dynamics of the 1054 UT March 22, 1979, substorm event: CDAW 6, *J. Geophys. Res.*, this issue.

Nishida, A., IMF control of the earth's magnetosphere, *Space Sci. Rev.*, *34*, 185, 1983.

Paschmann, G., N. Sckopke, and E. W. Hones, Jr., Magnetotail plasma observations during the 1054 UT substorm on March 22, 1979 (CDAW 6), *J. Geophys. Res.*, this issue.

Rostoker, G., Triggering of expansive phase intensifications of magnetospheric substorms by northward turnings of the interplanetary magnetic field, *J. Geophys. Res.*, *88*, 6981, 1983.

Spiro, R. W., and R. A. Wolf, Electrodynamics of convection in the inner magnetosphere, in *Magnetospheric Currents*, *Geophys. Monogr. Ser.*, vol. 28, edited by T. A. Potemra, p. 247, AGU, Washington, D. C., 1984.

Tsurutani, B. T., J. A. Slavin, Y. Kamide, R. D. Zwickl, J. H. King, and C. T. Russell, Coupling between the solar wind and the magnetosphere: CDAW 6, *J. Geophys. Res.*, this issue.

D. N. Baker and T. A. Fritz, Los Alamos National Laboratory, University of California, Los Alamos, NM 87545.

W. Baumjohann, Institut für extraterrestrische Physik, Max-Planck-Institut für Physik und Astrophysik, Garching, Federal Republic of Germany.

D. H. Fairfield, NASA Goddard Space Flight Center, Greenbelt, MD 20771.

Y. Kamide, Kyoto Sangyo University, Kyoto 603, Japan.

R. L. McPherron, University of California, Los Angeles, Los Angeles, CA 90024.

(Received March 2, 1984;
revised May 25, 1984;
accepted May 29, 1984.)